

Substellar Companions to Seven Evolved Intermediate-Mass Stars

Bun'ei SATO,¹ Masashi OMIYA,¹ Hiroki HARAKAWA,¹ Hideyuki IZUMIURA,^{2,3} Eiji KAMBE,² Yoichi TAKEDA,^{3,4}
Michitoshi YOSHIDA,⁵ Yoichi ITOH,⁶ Hiroyasu ANDO,^{3,4} Eiichiro KOKUBO^{3,4} and Shigeru IDA¹

¹*Department of Earth and Planetary Sciences, Tokyo Institute of Technology, 2-12-1 Ookayama, Meguro-ku, Tokyo 152-8551, Japan*

satobn@geo.titech.ac.jp

²*Okayama Astrophysical Observatory, National Astronomical Observatory of Japan, Kamogata, Okayama 719-0232, Japan*

³*The Graduate University for Advanced Studies, Shonan Village, Hayama, Kanagawa 240-0193, Japan*

⁴*National Astronomical Observatory of Japan, 2-21-1 Osawa, Mitaka, Tokyo 181-8588, Japan*

⁵*Hiroshima Astrophysical Science Center, Hiroshima University, Higashi-Hiroshima, Hiroshima 739-8526, Japan*

⁶*Graduate School of Science, Kobe University, 1-1 Rokkodai, Nada, Kobe 657-8501, Japan*

(Received ; accepted)

Abstract

We report the detections of substellar companions orbiting around seven evolved intermediate-mass stars from precise Doppler measurements at Okayama Astrophysical Observatory. σ UMa (G4 II-III) is a giant with a mass of $3.1 M_{\odot}$ and hosts a planet with minimum mass of $m_2 \sin i = 4.1 M_J$ in an orbit with a period $P = 1630$ d and an eccentricity $e = 0.13$. This is the first planet candidate ($< 13 M_J$) ever discovered around stars more massive than $3 M_{\odot}$. σ CrB (K0 III) is a $2.1 M_{\odot}$ giant and has a planet of $m_2 \sin i = 1.5 M_J$ in a 187.8 d orbit with $e = 0.19$. This is one of the least massive planets ever discovered around $\sim 2 M_{\odot}$ stars. HD 5608 (K0 IV) is an $1.6 M_{\odot}$ subgiant hosting a planet of $m_2 \sin i = 1.4 M_J$ in a 793 d orbit with $e = 0.19$. The star also exhibits a linear velocity trend suggesting the existence of an outer, more massive companion. 75 Cet (G3 III:) is a $2.5 M_{\odot}$ giant hosting a planet of $m_2 \sin i = 3.0 M_J$ in a 692 d orbit with $e = 0.12$. The star also shows possible additional periodicity of about 200 d and 1880 d with velocity amplitude of $\sim 7\text{--}10 \text{ m s}^{-1}$, although these are not significant at this stage. ν Oph (K0 III) is a $3.0 M_{\odot}$ giant and has two brown-dwarf companions of $m_2 \sin i = 24 M_J$ and $27 M_J$, in orbits with $P = 530.3$ d and 3190 d, and $e = 0.126$ and 0.17, respectively, which were independently announced by Quirrenbach et al. (2011). The ratio of the periods is close to 1:6, suggesting that the companions are in mean motion resonance. We also independently confirmed planets around κ CrB (K0 III-IV) and HD 210702 (K1 IV), which had been announced by Johnson et al. (2008) and Johnson et al. (2007a), respectively. All of the orbital parameters we obtained are consistent with the previous results.

Key words: stars: individual: HD 5608 — stars: individual: 75 Cet — stars: individual: σ UMa — stars: individual: σ CrB — stars: individual: ν Oph — stars: individual: κ CrB — stars: individual: HD 210702 — planetary systems — techniques: radial velocities

1. Introduction

Intermediate-mass ($1.5\text{--}5 M_{\odot}$) stars have been gathering more attention of researchers as promising sites of planet formation. It is not only because some planetary systems were found around A-type dwarfs by direct imaging (e.g. Marois et al. 2008) but also intensive Doppler surveys of intermediate-mass giants and subgiants, which are “evolved counterparts of A-type dwarfs”, have unveiled remarkable properties of planets around them (e.g. Frink et al. 2002; Setiawan et al. 2005; Sato et al. 2008b; Sato et al. 2010; Hatzes et al. 2005; Hatzes et al. 2006; Johnson et al. 2011a; Lovis & Mayor 2007; Niedzielski et al. 2009b; Döllinger et al. 2009; de Medeiros et al. 2009; Wang et al. 2011; Omiya et al. 2011; Wittenmyer et al. 2011). About 50 substellar companions have been found around such evolved intermediate-mass stars, whose masses, semimajor axes, and eccentricities are ranging from 0.6 to $40 M_J$, from 0.08 to 6 AU, and from 0 to

0.5, respectively¹. The occurrence rate of giant planets increases as stellar mass at least up to $\sim 1.9 M_{\odot}$ ($\sim 10\text{--}20\%$; e.g. Johnson et al. 2007b; Bowler et al. 2010), and super-massive ($\gtrsim 5 M_J$) planets are more abundant around more massive ($\gtrsim 2 M_{\odot}$) giants (e.g. Lovis & Mayor 2007). Positive correlation between frequency of giant planets and stellar metallicity may exist in subgiants like in solar-type stars (Johnson et al. 2010) but not be seen in giants (e.g. Pasquini et al. 2007; Takeda et al. 2008). Semimajor-axis distribution of the planets is one of the most interesting features; almost all the planets found around intermediate-mass evolved stars reside in orbits with semimajor axis larger than 0.6 AU (e.g. Johnson et al. 2007a; Sato et al. 2008a), while many short-period planets exist around low-mass FGK dwarfs. Multi-planet systems have also been found around evolved intermediate-mass stars including candidates in mean motion resonance (MMR;

¹ see e.g. <http://exoplanet.eu>

Niedzielski et al. 2009a; Johnson et al. 2011b; Quirrenbach et al. 2011). All the properties give us deep insight into formation and evolution of substellar companions around intermediate-mass stars.

We here report the detections of new substellar companions around evolved intermediate-mass stars emerged from the Okayama Planet Search Program (Sato et al. 2005). The program has been regularly monitoring radial velocities (RVs) of about 300 intermediate-mass GK giants since 2001 at Okayama Astrophysical Observatory (OAO) and announced 9 planets and 1 brown dwarf so far (Sato et al. 2003; Sato et al. 2007; Sato et al. 2008a; Sato et al. 2008b; Liu et al. 2008). We also discovered 3 planets and 3 brown-dwarf candidates around GK giants using 2.16m telescope at Xinglong observatory in China, 1.8m telescope at Bohyunsan Optical Astronomy Observatory in Korea, and Subaru 8.2m telescope in Hawaii as well as OAO 1.88m telescope under the framework of East-Asian Planet Search Network (Liu et al. 2009; Omiya et al. 2009; Omiya et al. 2011; Sato et al. 2010; Wang et al. 2011).

Rest of the paper is organized as follows. We describe the observations in section 2 and the stellar properties are presented in section 3. Analyses of RV, linear trend, period search, orbital solution, and line shape variation are described in section 4 and the results are presented in section 5. Section 6 is devoted to summary and discussion.

2. Observation

All of the observations were made with the 1.88 m telescope and the HIGH Dispersion Echelle Spectrograph (HIDES; Izumiura 1999) at OAO. In 2007 December, HIDES was upgraded from single CCD (2K×4K) to a mosaic of three CCDs. The upgrade enabled us to obtain spectra covering a wavelength range of 3750–7500Å using a red cross-disperser, which is about three times wider than before the upgrade.

For precise RV measurements, we used an iodine absorption cell (I₂ cell; Kambe et al. 2002), which provides a fiducial wavelength reference in a wavelength range of 5000–5800Å (covered by the middle CCD after the upgrade in 2007 December). A slit width is set to 200 μm (0.76'') giving a spectral resolution ($R = \lambda/\Delta\lambda$) of 67000 by about 3.3 pixels sampling. We can typically obtain a signal-to-noise ratio $S/N > 200 \text{ pix}^{-1}$ for a $V < 6.5$ star with an exposure time shorter than 30 min. The reduction of echelle data (i.e. bias subtraction, flat-fielding, scattered-light subtraction, and spectrum extraction) is performed using the IRAF² software package in the standard way.

3. Stellar Properties

Takeda et al. (2008) derived atmospheric parameters (effective temperature T_{eff} , surface gravity $\log g$, micro-turbulent velocity v_t , and Fe abundance $[\text{Fe}/\text{H}]$) of all

the targets for Okayama Planet Search Program based on the spectroscopic approach using the equivalent widths of well-behaved Fe I and Fe II lines of iodine-free stellar spectra. Details of the procedure and resultant parameters are presented in Takeda et al. (2002) and Takeda et al. (2008).

They also determined the absolute magnitude M_V of each star from the apparent V -band magnitude and Hipparcos parallax π (ESA 1997) taking account of correction of interstellar extinction A_V based on Arenou et al. (1992)'s table. The bolometric correction $B.C.$ was estimated based on the Kurucz (1993)'s theoretical calculation. With use of these parameters and theoretical evolutionary tracks of Lejeune & Schaerer (2001), the luminosity L and mass M of each star were obtained. The stellar radius R was estimated using the Stefan-Boltzmann relationship and the measured L and T_{eff} . The stars presented herein are plotted on the HR diagram in Figure 1 and their properties are summarized in Table 1.

The uncertainties for atmospheric and physical parameters of the stars were also derived by Takeda et al. (2008) and we quoted the values in Table 1. Since details of the procedure are described in Takeda et al. (2008), we here briefly summarize it. The uncertainties of $[\text{Fe}/\text{H}]$, T_{eff} , $\log g$, and v_t presented in the table are internal statistical errors for a given data set of Fe I and Fe II line equivalent widths (see subsection 5.2 of Takeda et al. 2002). Since these parameter values are sensitive to slight changes in the equivalent widths as well as to the adopted set of lines (Takeda et al. 2008), realistic uncertainties may be by a factor of ~ 2 –3 larger than these estimates from a conservative point of view (e.g., 50–100 K in T_{eff} , 0.1–0.2 dex in $\log g$). Therefore the ranges of stellar mass were obtained by perturbing the values of $\log L$, $\log T_{\text{eff}}$, and $[\text{Fe}/\text{H}]$ interchangeably by typical amounts of uncertainties; $\Delta \log L$ corresponding to parallax errors given in the Hipparcos catalog, $\Delta \log T_{\text{eff}}$ of ± 0.01 dex almost corresponding to $\sim \pm 100$ K, and $\Delta [\text{Fe}/\text{H}]$ of ± 0.1 dex. Similarly, the error in R was evaluated from $\Delta \log L$ and $\Delta \log T_{\text{eff}}$ (see the section 3.2 and footnote 8 of Takeda et al. 2008 for the details of the procedure). The resulting mass value may also appreciably depend on the chosen set of theoretical evolutionary tracks (e.g., the systematic difference as large as $\sim 0.5 M_{\odot}$ for the case of metal-poor tracks between Lejeune & Schaerer 2001 and Girardi et al. 2000.; see also footnote 3 in Sato et al. 2008a).

Hipparcos observations revealed photometric stability for the stars down to $\sigma_{\text{HIP}} = 0.004 - 0.008$ mag. Furthermore, all the stars show no significant emission in the core of Ca II HK lines as shown in Figure 2, suggesting that the stars are chromospherically inactive.

4. Analysis

4.1. Radial Velocity Analysis

For RV analysis, we basically adopted the modeling technique of an I₂-superposed stellar spectrum (star+I₂) detailed in Sato et al. (2002), which is based on the method by Butler et al. (1996). In the technique, a

² IRAF is distributed by the National Optical Astronomy Observatories, which is operated by the Association of Universities for Research in Astronomy, Inc. under cooperative agreement with the National Science Foundation, USA.

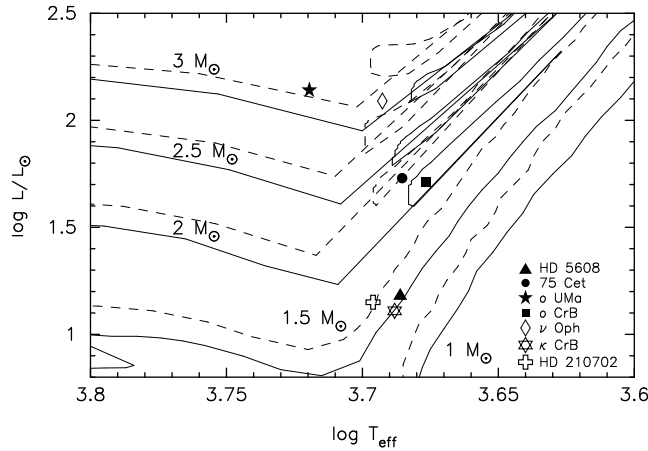


Fig. 1. HR diagram of the planet-harboring stars presented in this paper. Pairs of evolutionary tracks for Lejeune and Schaerer (2001) for stars with $Z = 0.02$ (solar metallicity; solid lines) and $Z = 0.008$ (dashed lines) of masses between 1 and $3 M_{\odot}$ are also shown.

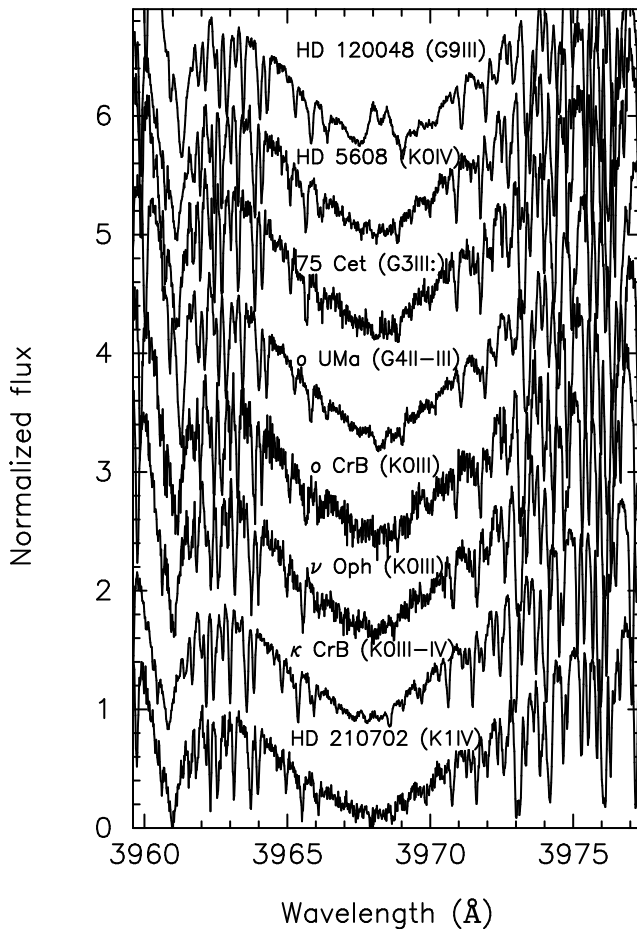


Fig. 2. Spectra in the region of Ca H lines. All of the stars show no significant core reversals in the lines compared to that in the chromospheric active star HD 120048, which shows velocity scatter of about 20 m s^{-1} . A vertical offset of about 0.8 is added to each spectrum.

star+I₂ spectrum is modeled as a product of a high resolution I₂ and a stellar template spectrum convolved with a modeled instrumental profile (IP) of the spectrograph. To obtain the stellar template, Sato et al. (2002) extracted a high resolution stellar spectrum from several star+I₂ spectra. However, we here used a stellar template that was obtained by deconvolving a pure stellar spectrum with the spectrograph IP estimated from an I₂-superposed B-star or Flat spectrum because we finally found that the overall precision in RV using the template thus obtained was slightly better than that based on the technique in Sato et al. (2002). We have now achieved a long-term Doppler precision of about $4\text{--}5 \text{ m s}^{-1}$ over a time span of 9 years. Measurement error was estimated from an ensemble of velocities from each of ~ 300 spectral regions (each $\sim 3\text{Å}$ long) in every exposure.

4.2. Linear Trend

We examined whether there is evidence of a linear trend in RVs with timescale much larger than the duration of observations. To address the significance of the velocity trend, we used the F -test in a similar way to that described by Cumming et al. (1999). The weighted sum of squares of residuals to the best-fit linear slope χ_{N-2}^2 is compared with the weighted sum of squares about the mean χ_{N-1}^2 . If there is no long-term trend in observed velocities and the residual follow Gaussian distribution, the statistic

$$F = (N - 2) \frac{\chi_{N-1}^2 - \chi_{N-2}^2}{\chi_{N-2}^2} \quad (1)$$

follows Fisher's F distribution with 1 and $N - 2$ degrees of freedom which measures how much the fit is improved by introducing the linear trend. Using this probability distribution, we can estimate the False Alarm Probability (FAP) that pure noise fluctuations would produce a linear velocity trend by chance. This method, however, assumes that the errors follow Gaussian distribution, which is not necessarily the case for the actual observations. Instead we here adopt so called a bootstrap randomization method to estimate FAP . In this approach, the observed RVs are randomly redistributed, keeping fixed the observation time. The major advantage of this method is that one can derive FAP without assuming any particular distribution of noise. For each star, we generated 10^5 fake datasets in this way, applied the same analysis to them, and obtained F -value by the equation (1). The frequency of fake datasets whose F exceeded the observed one was adopted as a FAP for the trend.

4.3. Period Search

To search for periodicity in RV data we performed a Lomb-Scargle periodogram analysis (Scargle 1982). To assess the significance of this periodicity, we estimate False Alarm Probability (FAP), using a bootstrap randomization method in which the observed RVs were randomly redistributed, keeping fixed the observation time. We generated 10^5 fake datasets in this way, and applied the same periodogram analysis to them. The frequency of

fake datasets which exhibit a periodogram power higher than the observed dataset is adopted as a *FAP* for the signal.

4.4. Orbital Solution

The best-fit Keplerian orbit for the data was derived using a Levenberg-Marquardt fitting algorithm (Press et al. 1989) to obtain a minimum chi-squared solution by varying the free parameters (orbital period P , time of periastron passage T_p , eccentricity e , velocity amplitude K_1 and argument of periastron ω for each companion). When we found a significant linear trend in observed RVs by the analysis described in section 4.2, we included the slope as a free parameter and simultaneously derived the best-fit trend and Keplerian orbit for the data.

Each star has stellar “jitter”, which is intrinsic variability in RV as a source of astrophysical noise such as stellar oscillation and chromospheric activity, and also unknown systematic measurement error. To account for the variability, we have quadratically added a jitter σ_{jitter} to the RV measurement uncertainties before performing the final least-squared fitting of the orbit so that the resultant reduced χ^2 would become unity.

The uncertainty for each orbital parameter was estimated using a bootstrap Monte Carlo approach, subtracting the theoretical fit, scrambling the residuals, adding the theoretical fit back to the residuals and then refitting.

4.5. Line Shape Analysis

We performed spectral line shape analysis based on high resolution stellar templates to investigate other possible causes of apparent RV variations such as pulsation and rotational modulation rather than orbital motion. Details of the analysis are described in Sato et al. (2007) and Sato et al. (2002), and here we briefly summarize the procedure.

At first, we extracted two stellar templates from five star+I₂ spectra at nearly the peak and valley phases of observed RVs for each star. Cross correlation profiles of the two templates were then calculated for about 40–100 spectral segments (4–5Å width each) in which severely blended lines or broad lines were not included. We calculated three bisector quantities for the derived cross correlation profile for each segment: the velocity span (BVS), which is the velocity difference between two flux levels of the bisector; the velocity curvature (BVC), which is the difference of the velocity span of the upper half and lower half of the bisector; and the velocity displacement (BVD), which is the average of the bisector at three different flux levels. Flux levels of 25%, 50%, and 75% of the cross correlation profile were used to calculate the above three bisector quantities. If both of the BVS and the BVC for stars are identical to zero and the average BVD agrees with the velocity difference between the two templates at the peak and valley phases of observed RVs ($\simeq 2K_1$), the cross correlation profiles can be considered to be symmetric and thus the observed RV variations are considered to be due to parallel shifts of the spectral lines, which is consistent with the planetary hypothesis.

5. Results

5.1. HD 5608 (HIP 4552)

We collected a total of 43 RV data of HD 5608 between 2003 February and 2011 November. The observed RVs are shown in Figure 3 and are listed in Table 2 together with their estimated uncertainties.

Based on the linear-trend test described in section 4.2, the star showed a significant linear trend of $-4.9 \text{ m s}^{-1} \text{ yr}^{-1}$ with *FAP* = 5×10^{-5} , suggesting the existence of an distant companion. After removing the trend from the observed RVs, Lomb-Scargle periodogram showed a significant peak around 766 day with a *FAP* < 10^{-5} . Simultaneous fitting of a single Keplerian model and a linear trend to the data yielded an orbital period of $P = 792.6 \pm 7.7$ days, a velocity semiamplitude $K_1 = 23.5 \pm 1.6 \text{ m s}^{-1}$, and an eccentricity $e = 0.190 \pm 0.061$ for the inner companion, and the acceleration of $\dot{\gamma} = -5.5 \text{ m s}^{-1} \text{ yr}^{-1}$ for the linear trend. When we adopt the stellar mass of $1.55 M_{\odot}$ for the star, we obtained a minimum mass of the inner companion $m_2 \sin i = 1.4 M_J$ and a semimajor axis $a = 1.9 \text{ AU}$. For the outer companion, we may give an order-of-magnitude relation between $\dot{\gamma}$ and the properties of the companion (e.g. Winn et al. 2009)

$$\frac{m_c \sin i_c}{a_c^2} \sim \frac{\dot{\gamma}}{G} = (0.031 \pm 0.003) M_J \text{ AU}^{-2} \quad (2)$$

where m_c is the companion mass, i_c is the orbital inclination, and a_c is the orbital radius.

The rms scatter of the residuals to the Keplerian fit was 6.3 m s^{-1} . The adopted stellar jitter for the star (see section 4.4) is $\sigma_{\text{jitter}} = 5.0 \text{ m s}^{-1}$, which is consistent with typical one for subgiants (Johnson et al. 2008), and we found no significant periodicity in the residuals. The resulting model is shown in Figure 3 overplotted on the velocities, whose error bars include the stellar jitter, and its parameters are listed in Table 9.

For line shape analysis, we extracted templates with velocity of $\sim 10 \text{ m s}^{-1}$ and ~ -20 – -30 m s^{-1} , and calculated cross correlation profile between them. As seen in Table 10, resultant BVS and BVC values of the cross correlation profiles did not show any significant variability, and BVD value agreed with the velocity difference between the two templates, which are consistent with the planetary hypothesis as the cause of the observed RV variations.

5.2. 75 Cet (HD 15779, HIP 11791)

We collected a total of 74 RV data of 75 Cet between 2002 February and 2011 December. The observed RVs are shown in Figure 4 and are listed in Table 3 together with their estimated uncertainties. Lomb-Scargle periodogram of the data exhibits a dominant peak at a period of 698 days with a *FAP* < 1×10^{-5} .

Single Keplerian model for the star yielded orbital parameters for the companion of $P = 691.9 \pm 3.6$ days, $K_1 = 38.3 \pm 2.0 \text{ m s}^{-1}$, and $e = 0.117 \pm 0.048$. Adopting a stellar mass of $2.49 M_{\odot}$, we obtain $m_2 \sin i = 3.0 M_J$ and $a = 2.1 \text{ AU}$ for the companion. The rms scatter of the residuals to the Keplerian fit is 10.8 m s^{-1} and the

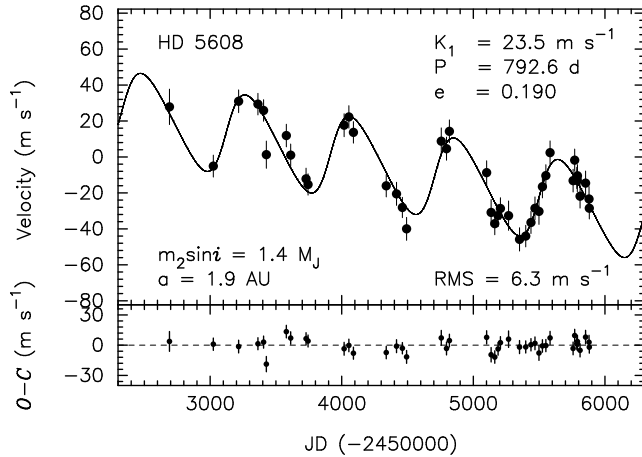


Fig. 3. *Top:* Radial velocities of HD 5608 observed at OAO. The Keplerian orbit with the linear trend is shown by the solid line. The error bar for each point includes the stellar jitter estimated in section 5.1. *Bottom:* Residuals to the orbital fit. The rms to the fit is 6.3 m s^{-1} .

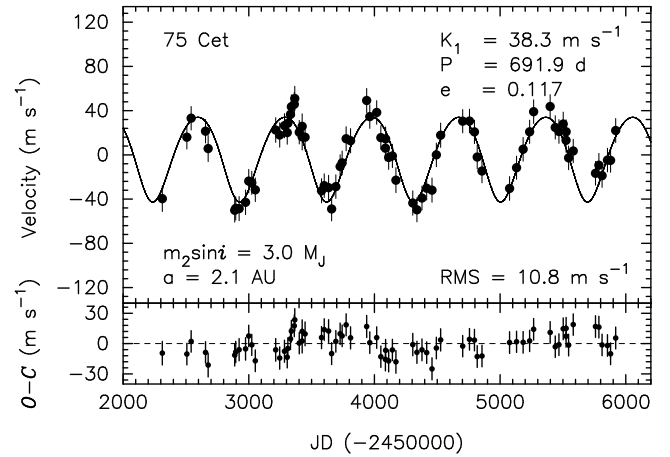


Fig. 4. *Top:* Radial velocities of 75 Cet observed at OAO. The Keplerian orbit is shown by the solid line. The error bar for each point includes the stellar jitter estimated in section 5.2. *Bottom:* Residuals to the Keplerian fit. The rms to the fit is 10.8 m s^{-1} .

reduced $\sqrt{\chi^2}$ was 2.7 when we adopted the measurement errors as weight of the least-squared fitting.

We performed periodogram analysis to the residuals and found possible peaks around 200 d and 1880 d (Figure 5). Although these periodicity is not significant at this stage ($FAP \sim 3 \times 10^{-3}$), Keplerian fitting yielded velocity semiamplitudes of $\sim 7 \text{ m s}^{-1}$ and $\sim 10 \text{ m s}^{-1}$ for the periodicity, respectively, which corresponds to $m_2 \sin i \sim 0.4 M_J$ and $1 M_J$, and $a \sim 0.9 \text{ AU}$ and $\sim 4 \text{ AU}$, respectively. Continuous monitoring of the star will enable us to validate the periodicity. We here have quadratically added a jitter of 10 m s^{-1} to the RV uncertainties to account for the RMS scatter to the single Keplerian model. The resulting model is shown in Figure 4 overlapped on the velocities, and its parameters are listed in Table 9.

We did not find any significant line-shape variability corresponding to the primary period of 692 d (Table 10), while those corresponding to the other possible periods were below the detection limit of the line shape analysis because of their low velocity amplitudes.

5.3. *o* UMa (HD 71369, HIP 41704)

We collected a total of 26 RV data of *o* UMa between 2003 December and 2011 March. The observed RVs are shown in Figure 6 and are listed in Table 4 together with their estimated uncertainties. Lomb-Scargle periodogram of the data exhibits a dominant peak at a period of 1575 days with a $FAP < 1 \times 10^{-5}$.

Single Keplerian model for the star yielded orbital parameters for the companion of $P = 1630 \pm 35$ days, $K_1 = 33.6 \pm 2.1 \text{ m s}^{-1}$, and $e = 0.130 \pm 0.065$. Adopting a stellar mass of $3.09 M_\odot$, we obtain $m_2 \sin i = 4.1 M_J$ and $a = 3.9 \text{ AU}$ for the companion. The rms scatter of the residuals to the Keplerian fit was 7.6 m s^{-1} . We found no significant periodicity in the residuals and then we adopted a stellar jitter $\sigma_{\text{jitter}} = 6.5 \text{ m s}^{-1}$ for the star. The resulting model is shown in Figure 6 overlapped on the velocities, and its

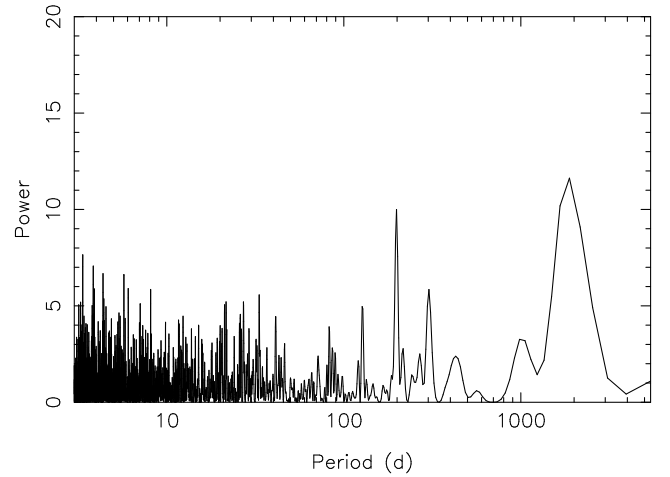


Fig. 5. Periodogram of the residuals to the Keplerian fit for 75 Cet. Possible peaks ($FAP \sim 0.003$) are seen at periods of about 200 and 1880 days.

parameters are listed in Table 9. We did not find any significant line shape variability for the star corresponding to the observed RV variations (Table 10).

5.4. *o* CrB (HD 136512, HIP 75049)

We collected a total of 85 RV data of *o* CrB between 2002 March and 2011 October. The observed radial velocities are shown in Figure 7 and are listed in Table 5 together with their estimated uncertainties. Lomb-Scargle periodogram of the data exhibits a dominant peak at a period of 187.7 days with a $FAP < 1 \times 10^{-5}$.

Single Keplerian model for the star yielded orbital parameters for the companion of $P = 187.83 \pm 0.54$ days, $K_1 = 32.25 \pm 2.8 \text{ m s}^{-1}$, and $e = 0.191 \pm 0.085$. Adopting a stellar mass of $2.13 M_\odot$, we obtain $m_2 \sin i = 1.5 M_J$ and $a = 0.83 \text{ AU}$ for the companion. The rms scatter

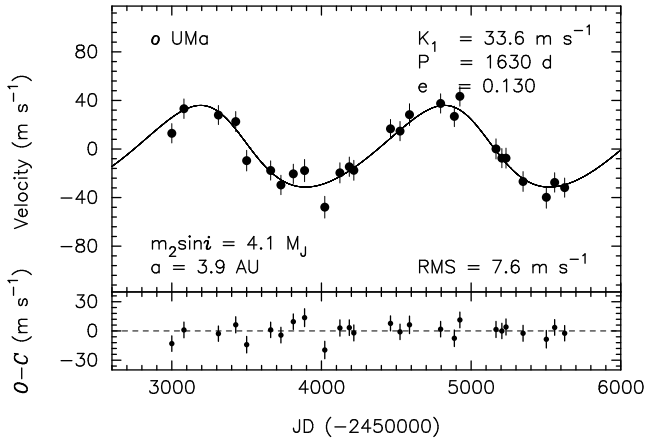


Fig. 6. *Top:* Radial velocities of *o* UMa observed at OAO. The Keplerian orbit is shown by the solid line. The error bar for each point includes the stellar jitter estimated in section 5.3. *Bottom:* Residuals to the Keplerian fit. The rms to the fit is 7.6 m s^{-1} .

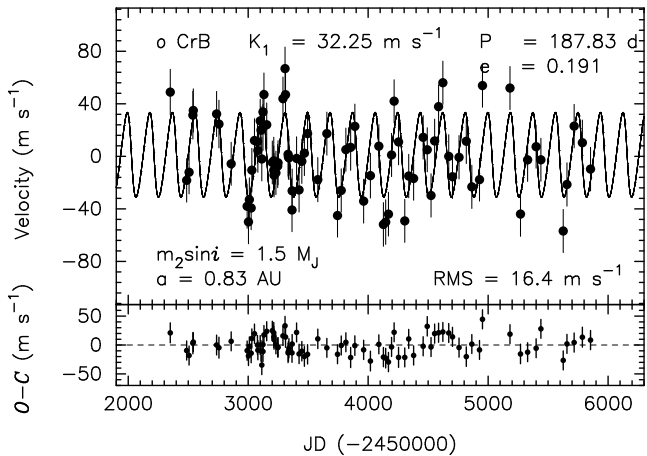


Fig. 7. *Top:* Radial velocities of *o* CrB observed at OAO. The Keplerian orbit is shown by the solid line. The error bar for each point includes the stellar jitter estimated in section 5.4. *Bottom:* Residuals to the Keplerian fit. The rms to the fit is 16.4 m s^{-1} .

of the residuals to the Keplerian fit is 16.4 m s^{-1} and the reduced $\sqrt{\chi^2}$ was 3.9 when we adopted the measurement errors as weight of the least-squared fitting, which may suggest existence of additional variability. However, we found no significant periodicity in the residuals at this stage and then we have quadratically added a jitter of 16.0 m s^{-1} to the RV uncertainties to account for the variations. The resulting Keplerian model is shown in Figure 7 and 8 overplotted on the velocities, and its parameters are listed in Table 9. We did not find any significant line shape variability for the star corresponding to the observed RV variations (Table 10).

5.5. ν Oph (HD 163917, HIP 88048)

Brown dwarf companions to ν Oph were reported by Quirrenbach et al. (2011) in a conference proceeding, al-

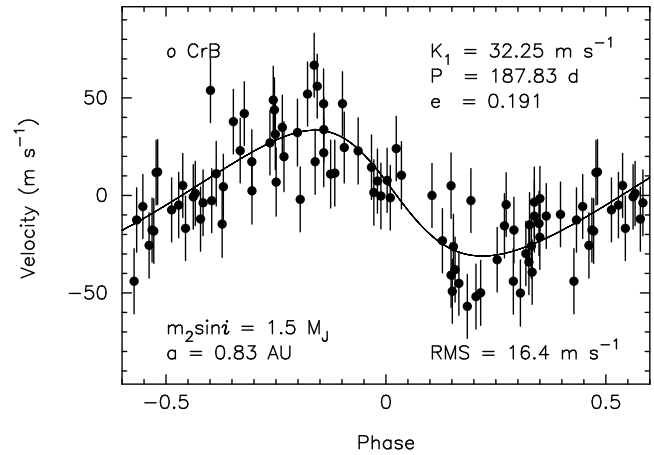


Fig. 8. Phased radial velocities of *o* CrB observed at OAO. The Keplerian orbit is shown by the solid line. The error bar for each point includes the stellar jitter estimated in section 5.4.

though details of the orbital parameters were not presented. We collected a total of 44 RV data of ν Oph between 2002 February and 2011 July. The observed RVs are shown in Figure 9 and are listed in Table 6 together with their estimated uncertainties.

Lomb-Scargle periodogram of the data exhibits a significant peak at a period of 526 days with a $FAP < 1 \times 10^{-5}$, and single Keplerian model for the star yielded orbital parameters for the companion of $P = 532$ days, $K_1 = 331 \text{ m s}^{-1}$, and $e = 0.15$. However, the rms scatter of the residuals to the fit was 99.4 m s^{-1} and the reduced $\sqrt{\chi^2}$ was 16.1, which suggested the existence of additional variability. Actually Lomb-Scargle periodogram of the residuals clearly showed a peak with a period of ~ 3000 d with a $FAP < 1 \times 10^{-5}$.

We performed a double Keplerian fitting to the data and obtained orbital parameters $P = 530.32 \pm 0.35$ days, $K_1 = 286.5 \pm 1.8 \text{ m s}^{-1}$, and $e = 0.1256 \pm 0.0065$ for the inner companion (ν Oph b), and $P = 3186 \pm 14$ days, $K_1 = 180.5 \pm 3.1 \text{ m s}^{-1}$, and $e = 0.165 \pm 0.013$ for the outer companion (ν Oph c). The rms scatter of the residuals to the double Keplerian fit is 7.8 m s^{-1} , and Lomb-Scargle periodogram of the residuals did not show any significant peaks. Then to account for the variations, we have quadratically added a jitter of 7.5 m s^{-1} to the RV uncertainties. All of the parameters are in agreement with those presented by Quirrenbach et al. (2011). Adopting a stellar mass of $3.04 M_\odot$, we obtain $m \sin i = 24 M_J$ and $a = 1.9 \text{ AU}$ for ν Oph b, and $m \sin i = 27.0 M_J$ and $a = 6.1 \text{ AU}$ for ν Oph c. The resulting Keplerian model is shown in Figure 9 and that for each companion is shown in Figure 10 overplotted on the velocities. The orbital parameters are listed in Table 9.

For line shape analysis, we extracted templates with velocity of $\sim 300 \text{ m s}^{-1}$ and $\sim -250 \text{ m s}^{-1}$, and calculated cross correlation profile between them. As seen in Table 10, non-detection of any significant variations in BVS and BVC values, and the BVD value agreeing with

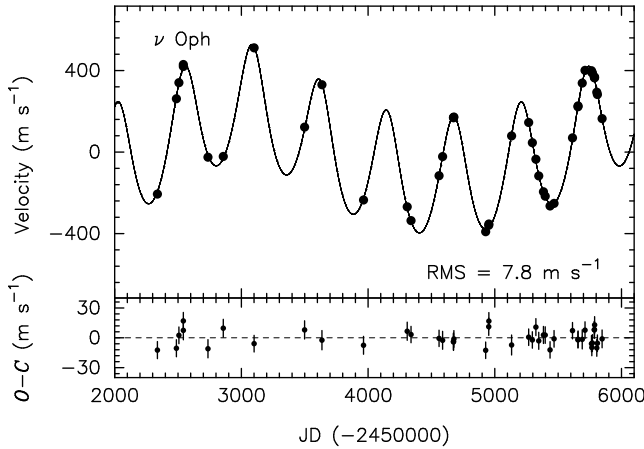


Fig. 9. *Top:* Radial velocities of ν Oph observed at OAO. The Keplerian orbit is shown by the solid line. The error bar for each point includes the stellar jitter estimated in section 5.5. *Bottom:* Residuals to the Keplerian fit. The rms to the fit is 7.8 m s^{-1} .

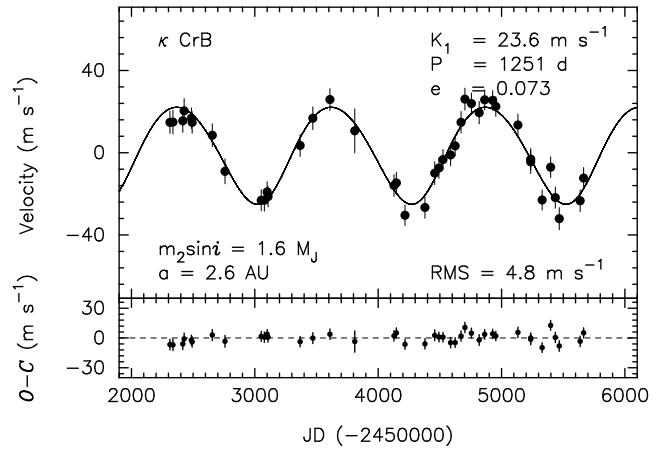


Fig. 11. *Top:* Radial velocities of κ CrB observed at OAO. The Keplerian orbit is shown by the solid line. The error bar for each point includes the stellar jitter estimated in section 5.6. *Bottom:* Residuals to the Keplerian fit. The rms to the fit is 4.8 m s^{-1} .

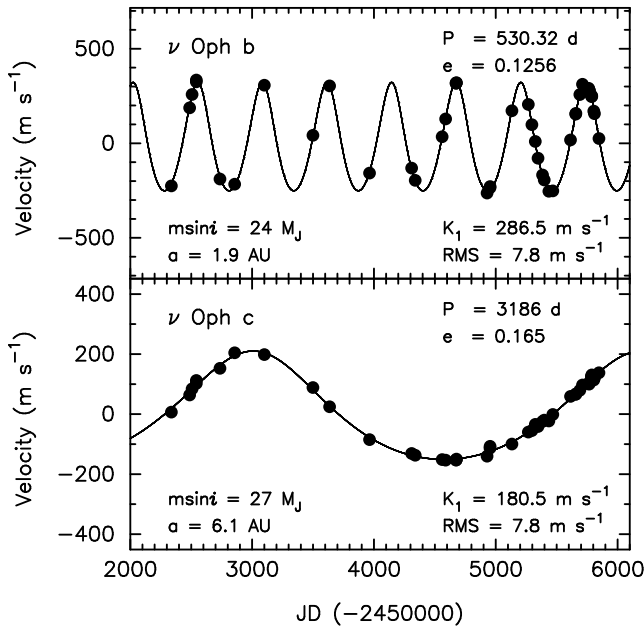


Fig. 10. Radial velocities of ν Oph observed at OAO. The Keplerian orbit is shown by the solid line. The error bar for each point includes the stellar jitter estimated in section 5.5. *Top:* Inner companion with the signal from the outer companion removed. *Bottom:* Outer companion with the signal from the inner companion removed.

the difference of the velocities between the two templates are consistent with the orbital-motion hypothesis as the cause of the observed RV variations.

5.6. κ CrB (HD 142091, HIP 77655) and HD 210702 (HIP 109577)

Planetary companions to κ CrB and HD 210702 were reported by Johnson et al. (2008) and Johnson et al. (2007a), respectively. We collected a total of 41 and 36

RV data of the stars between 2002 February and 2011 October, which is almost the same period of time as those of Johnson et al.'s. The observed RVs are shown in Figure 11 and 12 and are listed in Table 7 and 8, respectively, together with their estimated uncertainties. Our observed RVs for κ CrB can be well fitted by a single Keplerian orbit with $P = 1251 \pm 15$ days, $K_1 = 23.6 \pm 1.1 \text{ m s}^{-1}$, and $e = 0.073 \pm 0.049$. The RVs for HD 210702 can also be well fitted by a single Keplerian orbit with $P = 354.8 \pm 1.1$ days, $K_1 = 39.3 \pm 2.5 \text{ m s}^{-1}$, and $e = 0.094 \pm 0.052$. We here adopted a stellar jitter of 4.0 m s^{-1} and 4.5 m s^{-1} for κ CrB and HD 210702, respectively. These parameters are in good agreement with those obtained by Bowler et al. (2010). The resulting models are shown in Figure 11 and 12, and the parameters are listed in Table 9. Adopting stellar masses of $1.51 M_\odot$ and $1.68 M_\odot$ for κ CrB and HD 210702, respectively, we obtain $m_2 \sin i = 1.6 M_J$ and $a = 2.6 \text{ AU}$ for κ CrB b, and $m_2 \sin i = 1.9 M_J$ and $a = 1.2 \text{ AU}$ for HD 210702 b. We did not find any significant line shape variability for the stars corresponding to the observed RV variations (Table 10).

6. Summary and Discussion

We here reported the discoveries of planetary and brown-dwarf-mass companions to seven intermediate-mass subgiants and giants from Okayama planet search program: four new discoveries (HD 5608 b, 75 Cet b, o UMa b, o CrB b) and three independent confirmations of previous discoveries by other groups (ν Oph bc, κ CrB b, and HD 210702 b). The discoveries add to the recent growing population of substellar companions around evolved intermediate-mass stars.

HD 5608 b ($m_2 \sin i = 1.4 M_J$, $a = 1.9 \text{ AU}$) and 75 Cet b ($m_2 \sin i = 3.0 M_J$, $a = 2.1 \text{ AU}$) are typical planets orbiting intermediate-mass subgiants and giants in the point that the planets are $1\text{--}3 M_J$ and resides at $a \gtrsim 1 \text{ AU}$. HD 5608

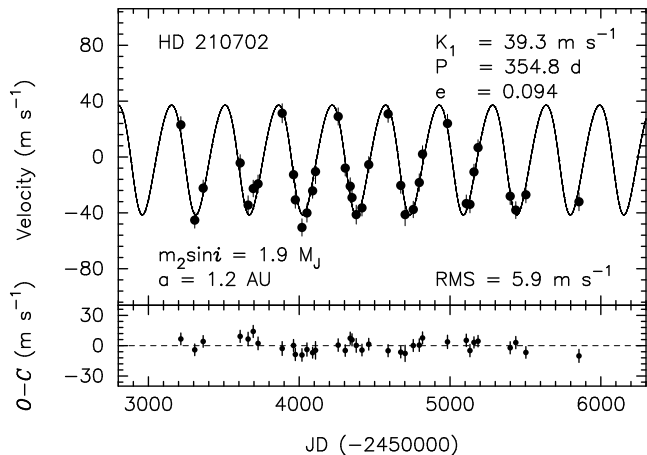


Fig. 12. *Top:* Radial velocities of HD 210702 observed at OAO. The Keplerian orbit is shown by the solid line. The error bar for each point includes the stellar jitter estimated in section 5.6. *Bottom:* Residuals to the Keplerian fit. The rms to the fit is 5.9 m s^{-1} .

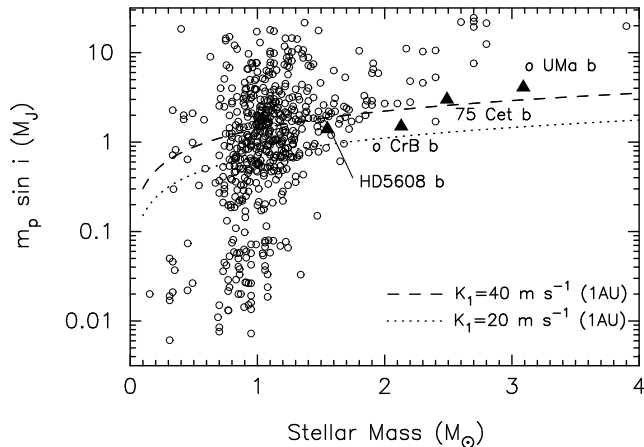


Fig. 13. Planetary mass distribution of exoplanets detected by RV methods against host star's mass. The data are from <http://exoplanets.eu>. Newly discovered planets (HD 5608 b, 75 Cet b, \circ UMa b, and \circ CrB b) are labeled by filled triangles. Dashed and dotted lines correspond to the velocity semi-amplitude of 40 and 20 m s^{-1} for a host star, respectively, imparted by a planet at 1 AU.

exhibits a linear trend in RV, suggesting the existence of an outer, more massive companion. The estimated mass of the outer companion based on equation (2) in section 5.1 exceeds $\sim 75 M_J$ if it orbits at $a \gtrsim 50 \text{ AU}$. 75 Cet also shows possible additional periodicity of about 200 d and 1880 d in RV with velocity semi-amplitude of $\sim 7\text{--}10 \text{ m s}^{-1}$. The significance of the periodicity should be validated by collecting more data.

\circ UMa b ($m_2 \sin i = 4.1 M_J$, $a = 3.9 \text{ AU}$) is the first planet candidate ($< 13 M_J$) ever discovered around stars with $\geq 3 M_\odot$ (see Fig. 13). Only brown-dwarf-mass companions had been found around such stars. The mass of $3 M_\odot$ corresponds to that for late-B to early-A type stars on the main sequence, which are normally rapid rotators with projected rotational velocity $v \sin i \gtrsim 100 \text{ km s}^{-1}$ and are also pulsating stars. It is thus quite difficult to find planets around them by Doppler methods. On the other hand, their evolved counter parts, GK giants, show RV jitter of $\sim 7 \text{ m s}^{-1}$ at most. Our discovery clearly shows that GK giants are suitable targets to access planets around such intermediate-mass stars.

\circ CrB b ($m_2 \sin i = 1.5 M_J$, $a = 0.83 \text{ AU}$) is one of the least massive planets ever discovered around clump giants, along with HD 100655 b ($m_2 \sin i = 1.7 M_J$, $a = 0.76 \text{ AU}$; Omiya et al. 2011; see Fig. 13). It is generally more difficult to detect such less massive planets around clump giants because of their larger stellar jitters compared with those of solar-type dwarfs and subgiants. \circ CrB shows RV semi-amplitude of 32 m s^{-1} , which is only twice of the RMS value of the jitter. Our discovery shows that we can detect such less massive planets even around clump giants if we collect a large number of data points.

ν Oph hosts two brown-dwarf-mass companions, ν Oph b ($m_2 \sin i = 24 M_J$) and ν Oph c ($m_2 \sin i = 27 M_J$). The ratio of the orbital period is close to 1:6 (530 d and 3186 d, respectively), suggesting that they are in MMR. Two such two-brown-dwarf systems have been previously

reported: one is a possible 3:2 MMR system around the clump giant BD+20 2457 (Niedzielski et al. 2009a) and the other is around a solar-type star HD 168443 (Marcy et al. 2001). Several scenarios are proposed for the formation of brown-dwarf-mass companions; gravitational collapse in protostellar clouds like stellar binary systems (Bonnell & Bastien 1992; Bate 2000) and gravitational instability in circumstellar disks (Boss 2000; Rice et al. 2003). Even core-accretion scenario could form such super-massive companions with $\gtrsim 10 M_J$ on a certain truncation condition for gas accretion (Ida & Lin 2004; Alibert et al. 2005; Mordasini et al. 2007). The existence of such two-companions in MMR suggests that they are formed in circumstellar disks by either gravitational instability or core-accretion, and then experience orbital migration. Detailed analysis of orbital stability for the system will be presented in a separate paper.

Figure 14 shows the semimajor-axis distribution of planets detected by RV method. It has been pointed out that almost no planets with $a \leq 0.6 \text{ AU}$ have been found around stars with masses $1.5\text{--}3 M_\odot$, and possible lack of planetary mass companions within 3 AU around $\sim 3 M_\odot$ was also pointed out (Omiya et al. 2009). \circ UMa b basically follows this trend; planets tend to stay at outer orbits as stellar mass increases. The semimajor axis distribution should be determined by the balance between some factors such as lifetime of a protoplanetary disk, efficiency of planet formation, and efficiency of orbital migration. From the numerical simulation by Currie (2009), the lack of inner planets around intermediate-mass stars (hereafter planet desert) can be reproduced if gas in a disk around intermediate-mass stars dissipates more quickly than around lower mass stars, and then planets can not migrate inward before the gas dissipation. In the case of $\sim 3 M_\odot$ stars, however, the existence or absence

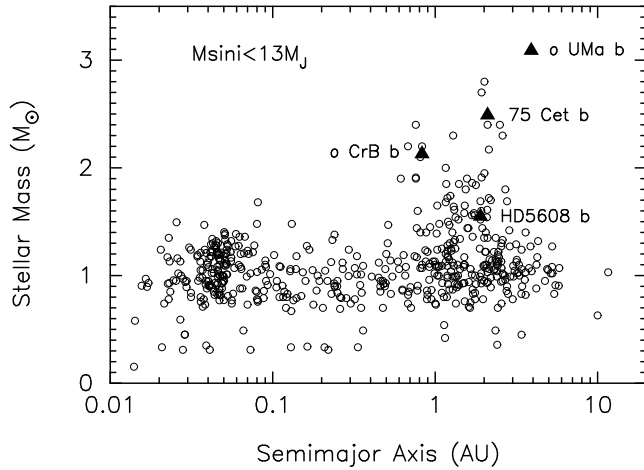


Fig. 14. Semimajor axis distribution of exoplanets ($m_2 \sin i < 13M_J$) detected by RV methods against host star's mass. The data are from <http://exoplanets.eu>. Newly discovered planets (HD 5608 b, 75 Cet b, o UMa b, and o CrB b) are labeled by filled triangles.

of the planet desert seems more sensitive to the above factors compared with $\sim 2 M_\odot$ stars; planets can form and migrate before the gas dissipation around $\sim 3 M_\odot$ stars depending on assumed lifetime of the disk. It is easier to explore inner planets around $\sim 3 M_\odot$ giants rather than around less massive ones because $\sim 3 M_\odot$ giants do not expand so largely at the tip of RGB. Then we need not consider planet engulfment by central stars except for very short-period ones, while planets within 0.4–1 AU around $\sim 2 M_\odot$ giants could have been engulfed during RGB phase of the central stars (Kunitomo et al. 2011). Planet searches around $\sim 3 M_\odot$ giants are thus highly encouraged.

Less massive planets ($\lesssim 2M_J$) around clump giants, such as o CrB b, should also be explored more intensively. Bowler et al. (2010) statistically showed that relatively higher-mass ($\gtrsim 2M_J$) planets tend to exist around intermediate-mass subgiants and excluded the same planet-mass distribution as that for solar-type stars. To push the detection limit from the current $K_1 \sim 40 \text{ m s}^{-1}$ ($\sim 2 M_J$ at $\sim 1 \text{ AU}$) down to $K_1 \sim 20 \text{ m s}^{-1}$ ($\sim 1 M_J$ at $\sim 1 \text{ AU}$) for clump giants ($\sim 2 M_\odot$) will allow us to directly compare the mass distribution of jovian planets for a wide range of host star's mass (see Fig. 13). We are now trying to do this by high cadence observations for a part of the sample of Okayama Planet Search Program. The results will be presented in a forthcoming paper.

This research is based on data collected at Okayama Astrophysical Observatory (OAO), which is operated by National Astronomical Observatory of Japan (NAOJ). We are grateful to all the staff members of OAO for their support during the observations. We thank students of Tokyo Institute of Technology and Kobe University for their kind help for the observations. BS was partly supported by MEXT's program "Promotion of

Environmental Improvement for Independence of Young Researchers" under the Special Coordination Funds for Promoting Science and Technology, and by Grant-in-Aid for Young Scientists (B) 20740101 from the Japan Society for the Promotion of Science (JSPS). HI is supported by Grant-In-Aid for Scientific Research (A) 23244038 from JSPS.

This research has made use of the SIMBAD database, operated at CDS, Strasbourg, France.

References

- Alibert, Y., Mordasini, C., Benz, W., Winisdoerffer, C. 2005, *A&A*, 434, 343
- Arenou, F., Grenon, M., & Gomez, A. 1992, *A&A*, 258, 104
- Bate, M. R. 2000, *MNRAS*, 314, 33
- Bonnell, I. & Bastien, P. 1992, *ApJ*, 401, 654
- Boss, A. P. 2000, *ApJ*, 536, L101
- Bowler, B.P., et al., *ApJ*, 710, 1365
- Butler, R. P., Marcy, G. W., Williams, E., McCarthy, C., Dosanjh, P., & Vogt, S. S. 1996, *PASP*, 108, 500
- Cumming, A., Marcy, G. W., & Butler, R. P., 1999, *ApJ*, 526, 890
- Currie, T. 2009, *ApJ*, 694, 171
- de Medeiros, J.R., et al., *A&A*, 504, 617
- Döllinger, M.P., Hatzes, A.P., Pasquini, L., Guenther, E.W., & Hartmann, M. 2009, *A&A*, 505, 1311
- ESA. 1997, *The Hipparcos and Tycho Catalogues* (ESA SP-1200; Noordwijk: ESA) *A&A*, 394, 5
- Frink, S., Mitchell, D.S., Quirrenbach, A., Fischer, D., Marcy, G.W., & Butler, R.P. 2002, *ApJ*, 576, 478
- Girardi, L., Bressan, A., Bertelli, G., & Chiosi, C. 2000, *A&AS*, 141, 371
- Hatzes, A.P., Guenther, E.W., Endl, M., Cochran, W.D., Döllinger, M.P., & Bedalov, A. 2005, *A&A*, 437, 743
- Hatzes, A.P., et al. 2006, *A&A*, 457, 335
- Ida, S. & Lin, D.N.C. 2004, *ApJ*, 616, 567
- Izumiura, H. 1999, in *Proc. 4th East Asian Meeting on Astronomy*, ed. P.S. Chen (Kunming: Yunnan Observatory), 77
- Johnson, J.A., et al. 2007a, *ApJ*, 665, 785
- Johnson, J.A., et al. 2007b, *ApJ*, 670, 833
- Johnson, J.A., et al. 2008, *ApJ*, 675, 784
- Johnson, J.A., et al. 2010, *PASP*, 122, 905
- Johnson, J.A., et al. 2011, *ApJS*, 197, 26
- Johnson, J.A., et al. 2011, *AJ*, 141, 16
- Kambe, E., et al. 2002, *PASJ*, 54, 865
- Kunitomo, M., Ikoma, M., Sato, B., Katsuta, Y., & Ida, S. 2011, *ApJ*, 737, 66
- Kurucz, R. L. 1993, *Kurucz CD-ROM*, No. 13 (Harvard-Smithsonian Center for Astrophysics)
- Liu, Y.-J., et al. 2008, *ApJ*, 672, 553
- Liu, Y.-J., Sato, B., Zhao, G., & Ando, H. 2009, *RAA*, 9, L1
- Lejeune, T., & Schaerer, D. 2001, *A&A*, 366, 538
- Lovis, C., & Mayor, M. 2007, *A&A*, 472, 657
- Marcy, G.W., et al., 2001, *ApJ*, 555, 418
- Marois, C., et al. 2008, *Science*, 322, 1348
- Mordasini, C., Alibert, Y., Benz, W., & Naef, D. 2007, in "Extreme Solar Systems", *ASP Conf. Ser. Vol. 398*, 235
- Niedzielski, A., Gozdziewski, K., Wolszczan, A., Konacki, M., Nowak, G., & Zielinski, P. 2009a, *ApJ*, 693, 276
- Niedzielski, A., Nowak, G., Adamow, M., & Wolszczan, A. 2009b, *ApJ*, 707, 768

- Omiya, M., et al., 2009, PASJ, 61, 825
Omiya, M., et al., 2011, PASJ, in press (arXiv:1111.3746v1)
Pasquini, L., et al. 2007, A&A, 473, 979
Press, W.H., Flannery, B.P., Teukolsky, S. A., Vetterling, W. T. 1989, "Numerical Recipe in C. The art of scientific computing", Cambridge Univ. Press
Quirrenbach, A., Reffert, S., & Bergmann, C. 2011, AIPC, 1331, 102
Rice, W.K.M., Armitage, P.J., Bonnell, I.A., Bate, M.R., Jeffers, S.V., & Vine, S.G., 2003, MNRAS, 346, L36
Sato, B., Kambe, E., Takeda, Y., Izumiura, H., & Ando, H. 2002, PASJ, 54, 873
Sato, B., et al. 2003, ApJ, 597, L157
Sato, B., Kambe, E., Takeda, Y., Izumiura, H., Masuda, S., & Ando, H. 2005, PASJ, 57, 97
Sato, B., et al. 2007, ApJ, 661, 527
Sato, B., et al. 2008a, PASJ, 60, 539
Sato, B., et al. 2008b, PASJ, 60, 1317
Sato, B., et al. 2010, PASJ, 62, 1063
Scargle, J. D. 1982, ApJ, 263, 835
Setiawan, J., et al. 2005, A&A, 437, 31
Takeda, Y., Ohkubo, M., & Sadakane, K. 2002, PASJ, 54, 451
Takeda, Y., Sato, B., & Murata, D., 2008, PASJ, 60, 781
Wang, L., et al., 2011, RAA, in press (arXiv:1110.0559v1)
Winn, J. N., Johnson, J.A., Albrecht, S., Howard, A.W., Marcy, G.W., Crossfield, I.J., & Holman, M.J., 2009, ApJL, 703, L99
Wittenmyer, R. A., Endl, M., Wang, L., Johnson, J. A., Tinney, C. G., & O'Toole, S. J. 2011, ApJ, 743, 184

Table 1. Stellar parameters

Parameter	HD 5608	75 Cet	<i>o</i> UMa	<i>o</i> CrB	ν Oph	κ CrB	HD 210702
Sp. Type	K0 IV	G3 III:	G4 II-III	K0 III	K0 III	K0 III-IV	[†] K1 IV
π (mas)	17.19 \pm 0.83	12.27 \pm 1.13	17.76 \pm 0.65	11.90 \pm 0.74	21.35 \pm 0.79	32.13 \pm 0.61	17.88 \pm 0.74
V	5.99	5.36	3.35	5.51	3.32	4.79	5.93
$B - V$	1.000	1.004	0.856	1.015	0.987	0.996	0.951
A_V	0.06	0.07	0.00	0.05	0.16	0.03	0.05
M_V	+2.11	+0.73	-0.40	+0.84	-0.19	+2.29	+2.14
$B.C.$	-0.31	-0.32	-0.19	-0.36	-0.28	-0.30	-0.27
T_{eff} (K)	4854 \pm 25	4846 \pm 18	5242 \pm 10	4749 \pm 20	4928 \pm 25	4877 \pm 25	4967 \pm 25
$\log g$ (cm s ⁻²)	3.03 \pm 0.08	2.63 \pm 0.05	2.64 \pm 0.03	2.34 \pm 0.06	2.63 \pm 0.09	3.21 \pm 0.08	3.19 \pm 0.08
v_t (km s ⁻¹)	1.08 \pm 0.07	1.26 \pm 0.08	1.51 \pm 0.07	1.39 \pm 0.06	1.46 \pm 0.10	1.04 \pm 0.09	1.10 \pm 0.08
[Fe/H] (dex)	+0.06 \pm 0.04	+0.00 \pm 0.04	-0.09 \pm 0.02	-0.29 \pm 0.03	+0.13 \pm 0.05	+0.10 \pm 0.04	+0.01 \pm 0.04
L (L_{\odot})	15.1	53.7	138	51.2	123	12.9	14.1
R (R_{\odot})	5.5 (5.1–5.9)	10.5 (9.5–11.5)	14.1 (13.2–15.1)	10.5 (9.8–11.2)	15.1 (14.1–16.2)	5.0 (4.8–5.2)	5.1 (4.8–5.5)
M (M_{\odot})	1.55 (1.32–1.74)	2.49 (2.22–2.51)	3.09 (3.02–3.16)	2.13 (1.90–2.14)	3.04 (2.98–3.10)	1.51 (1.32–1.70)	1.68 (1.50–1.84)
$v \sin i$ (km s ⁻¹)	1.37	1.77	3.83	2.30	3.21	1.21	1.99
σ_{HIP} (mag)	0.008	0.005	0.004	0.008	0.004	0.005	0.007

[†] The star is listed in the Hipparcos catalogue as a K1 III giant. But judged from the position of the star on the HR diagram (Figure 1), the star should be better classified as a less evolved subgiant.

Note – All of the values and uncertainties for atmospheric and physical parameters of the stars in this table are quoted by Takeda et al. (2008). The uncertainties of [Fe/H], T_{eff} , $\log g$, and v_t , are internal statistical errors and values in the parenthesis for stellar radius and mass correspond to the range of the values assuming more realistic uncertainties in $\Delta \log L$ corresponding to parallax errors in the Hipparcos catalog, $\Delta \log T_{\text{eff}}$ of ± 0.01 dex ($\sim \pm 100$ K), and $\Delta[\text{Fe}/\text{H}]$ of ± 0.1 dex. The resulting mass value may also appreciably depend on the chosen set of theoretical evolutionary tracks (e.g., the systematic difference as large as $\sim 0.5 M_{\odot}$ for the case of metal-poor tracks between Lejeune & Schaerer 2001 and Girardi et al. 2000.; see also footnote 3 in Sato et al. 2008a). Please see the section 3.2 and footnote 8 of Takeda et al. (2008) for the details of the procedure.

Table 2. Radial Velocities of HD 5608

JD (-2450000)	Radial Velocity (m s ⁻¹)	Uncertainty (m s ⁻¹)
2690.92265	27.9	8.5
3023.94225	-5.1	3.5
3216.26485	31.0	3.9
3363.07042	29.4	3.3
3405.95862	25.9	3.3
3426.91976	1.3	5.7
3579.20830	11.9	3.8
3612.20484	1.0	3.7
3729.06747	-12.2	3.2
3744.06021	-15.3	3.2
4018.28996	17.7	4.0
4054.11938	22.3	3.8
4089.07667	13.7	3.3
4338.27060	-16.0	3.6
4416.06811	-20.5	4.0
4461.00139	-28.1	2.6
4492.98453	-40.0	4.0
4756.22236	8.8	5.5
4796.02126	4.6	4.0
4818.10723	14.3	3.9
5101.24771	-8.7	4.3
5135.26954	-30.8	5.1
5162.97986	-37.1	3.7
5188.09633	-32.5	3.6
5205.95672	-28.7	3.3
5267.91741	-32.6	6.5
5351.29097	-45.8	4.1
5398.26283	-44.0	3.3
5438.06022	-36.4	3.6
5468.19458	-28.6	3.9
5499.02876	-30.3	5.3
5525.05040	-16.5	3.7
5550.99810	-10.4	3.4
5582.91808	2.4	4.2
5758.20356	-13.2	3.9
5770.25464	-1.8	3.6
5786.19124	-11.7	3.1
5790.26340	-13.1	3.7
5791.27944	-10.5	3.6
5811.29985	-21.8	4.3
5853.19065	-14.5	4.5
5879.07915	-23.4	4.8
5881.13007	-28.5	3.2

Table 3. Radial Velocities of 75 Cet

JD (-2450000)	Radial Velocity (m s ⁻¹)	Uncertainty (m s ⁻¹)
2311.96400	-39.6	5.9
2507.25607	16.0	3.9
2541.26302	33.2	3.7
2655.94596	21.4	3.6
2677.01385	5.7	6.2
2888.23459	-50.1	4.0
2896.19715	-48.4	3.4
2923.20790	-48.6	4.6
2974.17698	-42.9	4.9
2999.96007	-23.7	3.7
3023.90113	-25.3	3.1
3051.92008	-31.6	3.9
3214.27420	22.5	5.0
3246.32441	18.0	4.7
3284.20514	26.4	4.4
3306.14111	20.2	3.5
3311.15441	28.6	3.4
3332.08630	36.6	3.5
3339.20021	43.5	4.1
3362.02683	45.7	4.1
3366.04489	51.0	4.8
3401.90584	20.5	3.6
3424.90587	16.3	6.3
3424.92187	25.8	5.4
3447.93126	16.0	6.3
3579.24285	-32.5	4.4
3600.23799	-27.8	3.8
3635.25196	-29.7	5.0
3659.26573	-48.9	4.2
3693.17589	-28.8	3.9
3727.08594	-10.6	3.7
3743.05247	-7.2	3.8
3774.92427	14.6	4.4
3809.91688	12.8	4.6
3938.29450	49.2	4.4
3963.29661	34.6	3.8
4018.17496	38.3	3.8
4051.06681	15.6	3.5
4087.15142	6.0	5.5
4089.13018	14.5	4.1
4112.96188	-2.3	4.2
4142.97154	-1.0	3.4
4170.91468	-22.9	5.2
4305.26627	-43.5	4.7
4338.25207	-49.6	4.5
4378.20983	-39.0	4.2
4416.05343	-30.2	3.7
4458.10607	-31.9	4.4
4493.00758	0.0	3.8
4526.92907	17.8	4.6
4702.30722	30.5	3.4
4756.19459	30.6	3.8
4796.06006	20.8	3.7
4818.04972	-1.9	4.0
4856.01989	-14.6	3.7

Table 3. (Continued.)

JD (-2450000)	Radial Velocity (m s ⁻¹)	Uncertainty (m s ⁻¹)
5075.31961	-30.4	4.0
5131.15632	-11.6	3.2
5183.04922	5.1	3.8
5234.98763	20.8	3.5
5266.91271	39.1	3.8
5398.29099	43.8	3.9
5439.25969	24.8	3.5
5468.17983	21.2	3.9
5502.14696	27.9	4.0
5525.07454	13.2	4.2
5525.20750	20.9	4.2
5545.09659	-2.7	3.9
5581.98008	3.5	3.6
5759.28687	-16.7	3.8
5786.29592	-9.4	3.9
5811.27161	-18.8	3.7
5854.18481	-4.7	3.8
5879.12898	-5.0	4.1
5920.00604	22.0	4.2

Table 4. Radial Velocities of *o* UMa

JD (-2450000)	Radial Velocity (m s ⁻¹)	Uncertainty (m s ⁻¹)
3000.21377	12.9	4.6
3081.12751	33.2	4.8
3311.25752	28.0	4.4
3427.12651	22.6	5.1
3500.01480	-9.6	5.5
3660.31478	-17.7	4.5
3729.21876	-29.6	4.7
3812.09846	-20.4	4.6
3886.96433	-17.7	6.5
4022.32303	-47.9	6.2
4123.15218	-19.6	5.2
4186.04763	-14.6	4.6
4216.06204	-17.5	5.0
4461.33804	16.6	4.1
4525.12025	14.7	4.6
4587.94612	28.3	6.3
4796.33191	37.5	4.6
4887.99762	26.9	5.4
4925.03379	43.4	4.8
5166.10163	0.1	5.1
5205.19728	-7.5	4.5
5233.13003	-7.5	5.1
5346.97821	-26.8	5.0
5502.24894	-39.8	6.2
5558.23852	-27.5	4.7
5625.05259	-31.8	4.5

Table 5. Radial Velocities of α CrB

JD (-2450000)	Radial Velocity (m s ⁻¹)	Uncertainty (m s ⁻¹)
2350.23364	48.9	6.7
2487.03829	-18.3	4.3
2507.02176	-12.1	4.0
2538.95959	31.3	8.7
2541.92576	34.9	3.9
2736.22496	32.2	6.2
2756.22924	24.6	8.6
2858.04958	-5.7	3.6
2991.38250	-38.0	4.8
3002.31699	-49.9	4.7
3009.35443	-33.0	4.4
3024.30929	-39.3	4.2
3030.33746	-10.6	4.6
3052.21246	12.0	4.6
3077.21046	11.1	4.2
3080.24297	4.4	4.6
3100.14408	27.0	3.9
3106.13778	19.9	8.1
3113.09319	-2.0	4.6
3123.13165	21.9	6.9
3123.15778	33.8	4.5
3131.12074	47.0	3.6
3154.07703	24.0	4.4
3201.02789	-4.7	3.4
3213.05306	-3.5	8.2
3213.06729	-10.6	9.2
3215.05894	-14.4	3.9
3231.05763	-12.6	4.1
3245.98782	-7.4	3.7
3248.99489	-5.0	5.2
3289.89738	43.9	3.8
3306.87783	66.8	3.7
3310.88572	46.9	8.0
3332.36721	1.5	5.0
3335.35492	-0.3	5.4
3339.37537	-1.2	4.2
3365.33383	-40.9	4.1
3366.33105	-26.3	4.6
3403.28149	-1.6	3.9
3424.19652	-25.6	5.1
3447.27715	-3.8	5.4
3468.13912	2.4	5.9
3495.12788	17.3	4.9
3580.01261	-17.7	5.3
3655.89792	17.3	3.5
3744.34486	-45.1	3.5
3775.29240	-26.0	3.9
3814.25797	5.1	3.8
3854.14773	6.8	7.1
3889.13885	22.8	5.7
3962.08374	-34.1	4.8
4018.91296	-14.7	5.9
4089.34917	7.7	3.8
4127.30504	-51.9	4.6
4146.27743	-50.1	5.7

Table 5. (Continued.)

JD (-2450000)	Radial Velocity (m s ⁻¹)	Uncertainty (m s ⁻¹)
4169.13495	-44.0	4.7
4195.24643	1.0	3.9
4216.18929	42.0	3.3
4253.06244	10.9	6.9
4305.03318	-49.2	3.7
4337.99685	-15.0	4.1
4378.91908	-16.9	4.3
4458.35903	14.4	4.2
4492.34343	5.0	5.0
4524.27230	-29.8	3.9
4554.21774	11.7	4.4
4587.19292	37.8	4.3
4623.01424	56.0	3.6
4672.00836	-0.0	3.8
4702.95761	-15.6	4.0
4757.89315	-0.7	4.2
4818.34183	11.4	5.6
4864.31216	-23.2	3.9
4928.13244	-17.8	3.5
4953.09860	53.8	4.0
5182.37706	52.0	3.6
5270.27221	-44.0	5.5
5329.27285	-2.7	3.6
5400.04996	7.3	3.7
5439.96902	-2.6	3.6
5626.27038	-56.9	3.7
5657.24529	-21.4	4.1
5717.11504	23.0	4.3
5785.95886	10.3	6.5
5853.91399	-9.7	4.4

Table 6. Radial Velocities of ν Oph

JD (-2450000)	Radial Velocity (m s ⁻¹)	Uncertainty (m s ⁻¹)
2337.36482	-206.2	4.3
2487.10137	261.5	4.2
2507.07715	340.3	3.8
2541.95527	419.9	5.8
2541.95830	429.4	4.0
2736.30695	-25.2	5.3
2857.03714	-21.5	5.0
3100.27680	511.3	3.7
3499.17826	122.5	5.3
3636.02517	330.5	6.2
3963.95123	-235.1	4.9
4309.11301	-268.7	5.2
4338.99473	-336.4	3.4
4560.23968	-116.0	3.5
4588.26944	-22.3	5.0
4674.02304	169.2	4.1
4674.02538	168.7	4.1
4677.06734	171.7	3.8
4928.33015	-390.8	3.5
4952.30133	-359.5	4.5
4953.31022	-353.2	4.1
5132.93025	79.4	6.7
5267.33386	145.0	3.5
5296.32995	45.8	3.5
5324.28497	-35.2	4.0
5347.15367	-117.0	4.1
5384.18718	-194.7	4.2
5398.04796	-216.6	3.7
5436.02615	-264.5	3.5
5467.92821	-251.8	3.7
5613.38119	69.8	3.5
5656.34153	222.2	3.3
5657.34080	226.5	3.8
5690.21013	338.5	6.0
5712.15981	401.0	3.8
5763.07019	399.3	3.4
5766.07583	390.9	3.6
5770.06689	388.6	4.0
5784.95022	369.3	4.1
5787.00550	364.2	3.6
5788.00217	366.3	3.7
5804.92863	293.8	3.8
5809.97268	282.5	3.7
5846.91912	164.1	4.9

Table 7. Radial Velocities of κ CrB

JD (-2450000)	Radial Velocity (m s ⁻¹)	Uncertainty (m s ⁻¹)
2312.26533	14.8	3.6
2336.33946	14.9	4.1
2416.12452	15.5	4.0
2427.20074	20.4	4.4
2486.03119	16.8	3.1
2492.10142	14.7	3.4
2655.39085	8.5	3.9
2758.18803	-9.0	4.5
3052.22450	-23.1	3.2
3077.22294	-23.1	3.4
3100.19006	-19.1	3.0
3107.22020	-21.4	3.0
3367.32270	3.5	3.5
3470.23230	16.8	3.8
3609.05756	25.9	3.5
3810.20587	10.6	10.0
4128.36571	-16.0	3.5
4147.37825	-14.7	3.3
4217.18189	-30.4	3.0
4378.93344	-26.6	3.4
4458.36899	-9.9	3.8
4492.35201	-7.4	3.0
4525.33969	-3.4	2.8
4587.20318	-1.1	3.4
4624.06530	3.3	2.9
4672.01408	14.8	3.4
4702.96763	26.1	3.5
4755.90487	23.9	3.2
4818.37719	19.5	3.7
4863.38001	25.7	2.8
4928.14456	25.5	2.6
4953.14259	22.5	2.6
5132.89637	13.5	3.5
5236.30554	-4.4	4.0
5236.31346	-3.1	3.2
5329.28650	-23.0	2.8
5398.07959	-7.0	3.0
5435.97751	-21.8	3.3
5467.91961	-32.1	3.6
5637.20790	-23.4	3.5
5665.15483	-12.3	3.2

Table 8. Radial Velocities of HD 210702

JD (-2450000)	Radial Velocity (m s ⁻¹)	Uncertainty (m s ⁻¹)
3215.08376	23.0	3.7
3306.99833	-45.2	3.6
3362.91310	-22.3	3.6
3608.23193	-4.3	3.9
3661.15055	-34.4	4.9
3695.02464	-22.6	3.9
3726.91613	-19.2	4.4
3887.29767	31.3	5.2
3962.22805	-12.6	3.8
3974.12967	-30.7	4.0
4018.05863	-50.4	4.2
4051.04081	-40.1	4.8
4088.91609	-24.2	2.9
4107.92459	-10.5	7.4
4258.28341	29.0	4.2
4305.16396	-7.9	3.5
4338.13598	-20.9	4.1
4350.11134	-29.1	3.9
4378.17418	-41.3	5.1
4416.00348	-36.4	3.6
4460.96815	-5.5	3.6
4589.29655	30.8	4.0
4673.25542	-20.3	3.5
4702.27411	-41.2	6.6
4756.09323	-37.6	3.8
4795.97776	-18.3	4.3
4817.97314	2.1	3.9
4983.27072	24.0	4.8
5108.06283	-33.3	4.1
5132.05624	-33.9	4.1
5159.05429	-10.7	3.2
5185.87590	6.7	3.4
5399.16553	-28.1	3.9
5436.27068	-38.1	4.1
5503.00859	-27.0	3.7
5855.07749	-32.1	4.6

Table 9. Orbital Parameters

Parameter	HD 5608 b	75 Cet b	<i>o</i> UMa b	<i>o</i> CrB b	ν Oph b	ν Oph c	κ CrB b	HD 210702 b
P (days)	792.6±7.7	691.9±3.6	1630±35	187.83±0.54	530.32±0.35	3186±14	1251±15	354.8±1.1
K_1 (m s ⁻¹)	23.5±1.6	38.3±2.0	33.6±2.1	32.25±2.8	286.5±1.8	180.5±3.1	23.6±1.1	39.3±2.5
e	0.190±0.061	0.117±0.048	0.130±0.065	0.191±0.085	0.1256±0.0065	0.165±0.013	0.073±0.049	0.094±0.052
ω (deg)	269±22	165±28	58±42	79±36	9.6±3.8	4.6±4.5	210±51	126±47
T_p (JD-2,450,000)	2327±61	2213±54	3400±170	2211±17	2034.2±6.6	3038±38	1860±180	2205±45
$\dot{\gamma}$ (m s ⁻¹ yr ⁻¹)	-5.51±0.45	0 (fixed)	0 (fixed)	0 (fixed)	0 (fixed)	0 (fixed)	0 (fixed)	0 (fixed)
$a_1 \sin i$ (10 ⁻³ AU)	1.68±0.11	2.42±0.13	5.00±0.33	0.547±0.043	13.853±0.090	52.13±0.85	2.71±0.14	1.277±0.085
$f_1(m)$ (10 ⁻⁷ M_\odot)	0.0101±0.0020	0.0395±0.0062	0.063±0.012	0.0062±0.0016	12.61±0.25	18.62±0.89	0.0169±0.0025	0.0221±0.0046
$m_2 \sin i$ (M_J)	1.4	3.0	4.1	1.5	24	27	1.6	1.9
a (AU)	1.9	2.1	3.9	0.83	1.9	6.1	2.6	1.2
N_{obs}	43	74	26	85	44	44	41	36
RMS (m s ⁻¹)	6.3	10.8	7.6	16.4	7.8	7.8	4.8	5.9
[†] Reduced $\sqrt{\chi^2}$	1.7	2.7	1.6	3.9	2.2	2.2	1.6	1.6
σ_{jitter} (m s ⁻¹)	5.0	10	6.5	16	7.5	7.5	4.0	4.5

[†] The value without taking account of stellar jitter σ_{jitter}

Table 10. Bisector Quantities

Bisector Quantities	HD 5608	75 Cet	<i>o</i> UMa	<i>o</i> CrB	ν Oph	κ CrB	HD 210702
Bisector Velocity Span (BVS) (m s^{-1})	6.0 \pm 4.7	-5.8 \pm 4.3	-3.3 \pm 5.5	5.6 \pm 6.5	7.2 \pm 5.7	-4.7 \pm 3.9	-8.2 \pm 6.7
Bisector Velocity Curve (BVC) (m s^{-1})	3.1 \pm 3.4	3.4 \pm 2.2	0.4 \pm 3.8	0.4 \pm 3.6	-5.9 \pm 3.4	3.9 \pm 2.5	-1.4 \pm 4.5
Bisector Velocity Displacement (BVD) (m s^{-1})	-41 \pm 11	-71 \pm 9	-40 \pm 11	-77 \pm 12	-570 \pm 10	-31 \pm 7	-37 \pm 13